Topological spin Hall effect resulting from magnetic skyrmions

Gen Yin, Yizhou Liu, Yafis Barlas, Jiadong Zang, and Roger K. Lake

Topological Spin Hall Effect Resulting From Magnetic Skyrmions

Gen Yin,[1, *] Yizhou Liu,[1] Yafis Barlas,[1, 2] Jiadong Zang,[3, †] and Roger K. Lake[1, ‡]

[1]*Department of Electrical Engineering, University of California, Riverside, CA 92521-0204, USA*
[2]*Department of Physics and Astronomy, University of California, Riverside, CA 92521-0204, USA*
[3]*Department of Physics and Astronomy, Johns Hopkins University, Baltimore, MD 21218, USA*

The intrinsic spin Hall effect (SHE) originates from the topology of the Bloch bands in momentum space. The duality between real space and momentum space calls for a spin Hall effect induced from a real space topology in analogy to the topological Hall effect (THE) of skyrmions. We theoretically demonstrate the topological spin Hall effect (TSHE) in which a pure transverse spin current is generated from a skyrmion spin texture.

Transverse spin accumulation in semiconductors due to extrinsic spin-orbit scattering was first predicted by Dyakonov and Perel [1, 2]. Strong spin-orbit coupling (SOC) of the disorder scatters different spins in opposite directions leading to a non-zero transverse spin current perpendicular to the charged current. Evidence of the predicted asymmetric scattering of different spins was later observed in optical [3] and photovoltaic [4] experiments. Hirsch named this phenomenon the 'spin Hall effect' (SHE) and proposed that the chargeless transverse spin current can be transferred back to a Hall voltage using an inverse SHE measurement [5]. Later theoretical studies predicted an intrinsic contribution to the SHE in the presence of SOC due to the topological property of the Bloch states at the Fermi surface [6–10]. Direct observations of the SHE have been experimentally achieved in semiconductors using Kerr rotation microscopy[11, 12].

In magnetic materials, SOC can lead to a non-linear contribution to classical Hall signal[13–15]. The non-linearity, which is proportional to the magnetization, is a result of the transverse accumulation of itinerant majority spins resulting in the anomalous Hall effect (AHE) [16]. Similar to the SHE, the AHE can result from intrinsic or extrinsic mechanisms. The intrinsic contribution to the AHE is related to the Berry curvature of the Fermi surface which is determined by the topological nature of the Bloch bands [15, 17].

Both the intrinsic AHE and the intrinsic SHE result from a non-trivial topology in momentum space. Similarly, a Hall effect in a magnetic system can result from a non-trivial topology in real-space [18]. An electron hopping through magnetic sites with a chiral texture acquires a Berry phase and experiences an emergent gauge field during transport [19]. The emergent gauge field generates a Hall voltage that does not originate from SOC, and it is usually referred to as the 'topological Hall effect' (THE) [20]. Recently, skyrmion lattices, which are topologically non-trivial chiral spin textures, have been observed in helical magnets [21–23]. The measured Hall signal resulting from the THE is a signature of the skyrmion phase in many B20 magnetic compounds [24–27].

In the adiabatic limit, each electron spin passing through a single skyrmion has its spin aligned with the direction of spatial magnetization of the skyrmion which generates an emergent gauge field of up to one flux quantum [23]. One flux quantum confined in the area of a single skyrmion corresponds to a gigantic effective field. Moreover, the direction of this effective field is opposite for opposite spins, so that opposite spins are deflected in opposite directions. This might separate the spin current from the charge current, generating an unconventional topological spin Hall effect (TSHE) which does not originate from band topology. Motivated by these possibilities, in this letter we theoretically investigate the THE and the TSHE resulting from a single magnetic skyrmion. The TSHE phenomenon discovered here can be explained in terms of a general physical picture that would apply equally well to a skyrmion lattice.

Due to the lack of periodicity, we apply the non-equilibrium Green's function method (NEGF) to simulate the coherent transport of itinerant spins traversing a single magnetic skyrmion [28]. The tight-binding electron Hamiltonian we employ is,

$$\mathbf{H}_{\mathrm{e}} = -J_{\mathrm{H}} \sum_i c_i^\dagger \boldsymbol{\sigma}_i c_i \cdot \mathbf{S}_i - t \sum_{\langle i,j \rangle} \left(c_i^\dagger c_j + \mathrm{h.c.} \right), \quad (1)$$

where $\boldsymbol{\sigma}_i$ is the spin of itinerant electrons, J_{H} is the Hunds' rule coupling, t is the nearest neighbor hopping, and $\mathbf{S}_i$ is the local magnetization. It has been previously discussed that the external magnetic field does not contribute much to the Hall effect, therefore we neglect its effect on the electron by taking the hopping parameter to be real [16]. Thus, the Hall signal observed in the following calculations is purely from the emergent gauge field of the skyrmion. The spin texture $\{\mathbf{S}_i\}$ contains a single skyrmion located at the center of a 4-terminal cross bar (as shown in Fig. 1). This texture is fully damped using the Landau-Lifshitz-Gilbert (LLG) equation with the magnetic Hamiltonian $H_{\mathrm{S}} = -J \sum_{\langle i,j \rangle} \mathbf{S}_i \cdot \mathbf{S}_j - D \sum_{\langle i,j \rangle} \hat{\mathbf{r}}_{i,j} \cdot \mathbf{S}_i \times \mathbf{S}_j - \sum_i \mathbf{h}_0 \cdot \mathbf{S}_i$. Here J is the nearest neighbor exchange coupling, D is the Dzyaloshinskii-Moriya interaction, and $\mathbf{h}_0$ is the external magnetic field perpendicular to the cross-bar plane. For simplicity we choose $D = J = h_0^z$. Periodic magnetic boundaries are applied at the terminals in order to mimic the semi-infinite ferromagnetic leads.
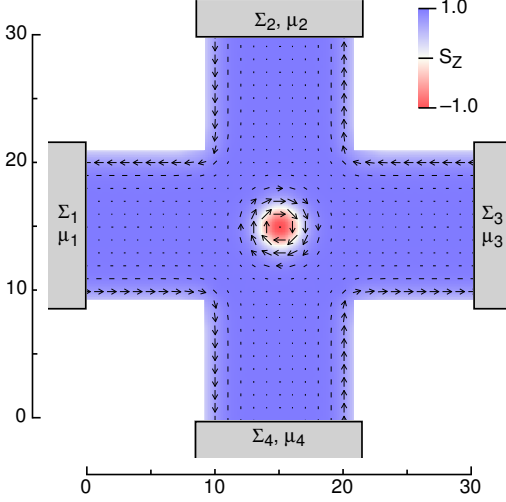
FIG. 1. (color online) The geometry of a 31×31 tight-binding cross bar. The arrows denote the in-plane component of the magnetization texture of a single skyrmion. The color plot demonstrates the S_z component. The four terminals are numbered clock-wise.

Other boundaries along the cross bar are taken as magnetic open boundaries, which gives large in-plane magnetization components at the edges. These boundary conditions have been applied to simulate helimagnetic ribbons [29]. The skyrmion at the center is generated by manually creating a unity topological charge and then relaxing the spin texture until the magnetic energy is stable. Details of the magnetic dynamical simulations can be found in Ref.[30]. It is assumed in the following that the electron current density is below the threshold for skyrmion motion [10, 29], so that the skyrmion is pinned within the central region.

For the electron transport calculation, semi-infinite boundary conditions for electron states are applied to the four terminals of the cross bar. Each terminal is assumed to be a thermal bath of carriers with chemical potential μ_m. The semi-infinite electrodes are included by adding self-energy terms, $\boldsymbol{\Sigma}_m = \mathbf{t}^\dagger \mathbf{g}_m^R \mathbf{t}$, to the terminal blocks of $\mathbf{H}_e$, where $\mathbf{g}_m^R$ is the surface Green's function of terminal m. The retarded Green's function of the device region bounded by the terminals is given by $\mathbf{G}^R = [\epsilon \mathbf{I} - \mathbf{H}_e - \sum_m \boldsymbol{\Sigma}_m]^{-1}$. In the linear response limit, the zero-temperature terminal currents, I_m, are given by $I_m = (e/h) \sum_n T_{m,n} \delta\mu_n$. $\delta\mu_n$ denotes the chemical potential shift due to an applied bias in terminal n, $(\delta\mu_n = \mu_n - \epsilon_F)$. $T_{m,n} = \text{Tr}\left[\boldsymbol{\Gamma}_m \mathbf{G}_{mn}^R \boldsymbol{\Gamma}_n \mathbf{G}_{mn}^A\right]$ $(m \neq n)$ is the transmission coefficient between terminal m and n, where $\mathbf{G}_{mn}^A = \mathbf{G}_{mn}^{R\dagger}$, and $\boldsymbol{\Gamma}_m = i\left(\boldsymbol{\Sigma}_m - \boldsymbol{\Sigma}_m^\dagger\right)$. At steady state, the charge current is conserved such that $T_{mm} = -\sum_{n \neq m} T_{mn}$. A Symmetric bias is applied between terminals 1 and 3, $\delta\mu_1 = -\delta\mu_3 = \delta\mu = 0.1 J_H$. Enforcing $I_2 = I_4 = 0$ in the Hall effect measure-

ment, the transverse Hall voltage can be solved as $\delta\mu_2 = \delta\mu\,(P - Q)/(P + Q)$ and $\delta\mu_4 = \delta\mu\,(R - S)/(R + S)$, where

$$
\begin{cases}
P = T_{21}T_{41} + T_{21}T_{42} + T_{21}T_{43} + T_{24}T_{41} \\
Q = T_{23}T_{41} + T_{23}T_{42} + T_{23}T_{43} + T_{24}T_{43} \\
R = T_{42}T_{21} + T_{21}T_{41} + T_{23}T_{41} + T_{24}T_{41} \\
S = T_{42}T_{23} + T_{21}T_{43} + T_{23}T_{43} + T_{24}T_{43}
\end{cases}
. \tag{2}
$$

Thus, the topological Hall angle can be evaluated as $\tan\theta_{\text{TH}} = E_H/E_x = (\mu_2 - \mu_4)/(\mu_1 - \mu_3)$.

Once $\delta\mu_m$ and I_m are obtained, then the total terminal spin current, $I_m^{S_\alpha}(\alpha = x, y, z)$, is evaluated from $I_m^{S_\alpha} = \frac{\hbar}{2}\text{Tr}\left[\boldsymbol{\sigma}_\alpha \mathbf{I}_m^{\text{neq}}\right]$, where $\boldsymbol{\sigma}_\alpha = \mathcal{I} \otimes \sigma_\alpha$ is the extended Pauli matrix and $\mathbf{I}_m^{\text{neq}}$ is the terminal current operator $\mathbf{I}_m^{\text{neq}} = \frac{i}{2\pi\hbar}\left[\delta\mathbf{G}_m^n \boldsymbol{\Sigma}_m^\dagger - \boldsymbol{\Sigma}_m \delta\mathbf{G}_m^n + \mathbf{G}_m^R \delta\boldsymbol{\Sigma}_m^{\text{in}} - \delta\boldsymbol{\Sigma}_m^{\text{in}}\mathbf{G}_m^A\right]$, $\delta\mathbf{G}_m^n = \sum_n \mathbf{G}_{m,n}^R \boldsymbol{\Gamma}_{n,n} \mathbf{G}_{n,m}^A \delta\mu_n$, and $\delta\boldsymbol{\Sigma}_m^{\text{in}} = \boldsymbol{\Gamma}_m(\epsilon_F)\delta\mu_m$. The intensity of the TSHE is described by the spin Hall angle, a renormalized ratio between the transverse spin current and the longitudinal charged current

$$
\theta_{\text{TSH}} = \left(\frac{2e}{\hbar}\right)\frac{\sigma_{xy}^{S_z}}{\sigma_{xx}} = \left(\frac{2e}{\hbar}\right)\frac{I_{42}^{s_z}}{I_{13}}, \tag{3}
$$

where $I_{13} = I_1 - I_3$, and $I_{42}^{S_z} = I_4^{S_z} - I_2^{S_z}$.

First, we study the THE and TSHE for the case of pure spin injection. By setting $t = 0.2J_H$, the tight-binding band-width is smaller than the spin splitting given by J_H. Therefore, no matter where the Fermi level lies, the electron injection does not mix different spins. The topological Hall angle θ_{TH} and topological spin Hall angle θ_{TSH} for different positions of ϵ_F are shown in Fig. 2(a) and (b), respectively. The corresponding surface density of states (DOS) that determines the type of current injection at terminal 1 is shown in Fig. 2(c). When the surface DOS is zero, the Fermi surface lies in the spin gap, injection is absent, and both θ_{TH} and θ_{TSH} are zero. As ϵ_F passes through the bands, pure spin injection gives a Hall angle up to ± 0.2 indicating the expected THE. The spin Hall angle θ_{TSH} of ± 0.005 is negligible. At $\epsilon_F = \pm J_H$, both θ_{TH} and θ_{TSH} change sign.

The sign change of the Hall angles can be explained by the spin and carrier-type composition of the injection from the ferromagnetic contacts. For each transport channel, a one-dimensional tight-binding chain gives a negative cosine electron band dispersion, which has a sign change of the effective mass at the band center. The effective mass (m^*) is positive at the bottom band-edge, and becomes negative at the top. When an up-spin electron with positive m^* is injected from terminal 1, it is scattered to the "right" due to the effect of the emergent gauge field generated by the skyrmion. This is denoted as scenario (I) in Fig. 2(d). Alternately when $m^* < 0$, an up-spin electron injected from terminal 1 is equivalent
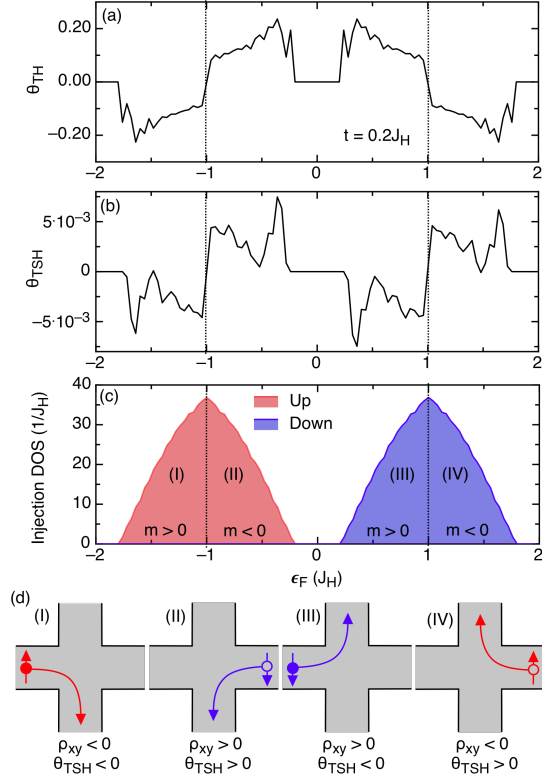
FIG. 2. (color online) THE and TSHE for the case of pure spin injection ($t = 0.2J_{\mathrm{H}}$). The (a) topological Hall angle θ_{TH} and the (b) topological spin Hall angle θ_{TSH} are shown as a function of ϵ_F. The surface density of states at terminal 1 is shown in (c). The four scenarios of different carrier-type and spin compositions are illustrated in (d).

FIG. 3. (color online) THE and TSHE in the case of mixed spin injection ($t = 1.5J_{\mathrm{H}}$). (a) and (b) demonstrate the values of θ_{TH} and θ_{TSH} for different positions of ϵ_F. The red dashed lines correspond to the case where the central skyrmion is removed. (c) is a plot of the surface DOS at terminal 1.

to a down-spin hole injected from terminal 3. Since the spin scattering due to the skyrmion is anti-symmetric, the down-spin hole is scattered to its "left" as denoted by scenario (II). In a multi-channel scenario due to the transverse confinement, the tight-binding band splits into several sub-bands. Thus, the number of the electron bands and the hole bands crossing the Fermi level changes at different positions of ϵ_F. As ϵ_F moves from the bottom band-edge to the band-center, the number of electron bands crossing ϵ_F decreases, while the number of hole bands increases as depicted in Fig. 2(c). Right at the band-center, the electrons and holes are equal, indicating an equal contribution from both scenarios (I) and (II), which leads to a cancellation of both θ_{TH} and θ_{TSH}. Further increasing ϵ_F, scenario (II) starts to dominate such that θ_{TH} and θ_{TSH} change sign. Similar arguments can be applied to scenario (III) and (IV) for the down-spin case (see Fig. 2(d)).

Semiclassically, the relative strength of THE to the TSHE can understood as a cancellation of the transverse electric field due to charge accumulation at contacts (2) and (4) with the gauge field of the skyrmion. In all of these pure-spin injection scenarios, the spin current is
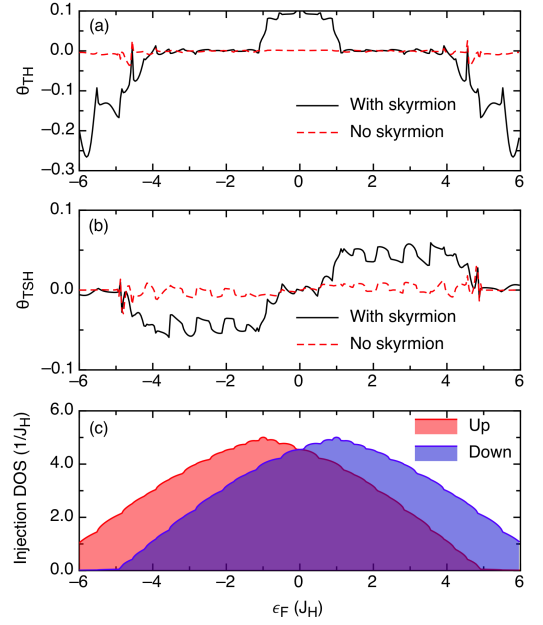
carried by charge which leads to a transverse accumulation of charge resulting in a Hall voltage and hence a THE. Since the transverse electric field cancels the Lorentz force given by the emergent gauge field of the skyrmion, a continuous spin current is suppressed at the steady state, making the TSHE insignificant. However, an order-of-magnitude increase in θ_{TSH} can be achieved in the case of mixed spin injection which we discuss next.

To simulate mixed spin injection, the hopping term is increased to $t = 1.5J_{\mathrm{H}}$ such that the injection band-widths of each spin are enlarged and overlap in some range of ϵ_F. The calculated values of the θ_{TH} and θ_{TSH} are shown in Fig. 3, along with the corresponding results in the absence of a skyrmion for comparison. For energies in the range of $-4.5J_{\mathrm{H}} < \epsilon_F < -J_{\mathrm{H}}$ and $J_{\mathrm{H}} < \epsilon_F < 4.5J_{\mathrm{H}}$, θ_{TH} vanishes to ~ 0, whereas θ_{TSH} increases by approximately an order of magnitude compared to the case of pure-spin injection. Additionally, in the energy range $-J_{\mathrm{H}} < \epsilon_F < J_{\mathrm{H}}$, the Hall angle θ_{H} corresponding to the THE is finite and roughly the same order as that in the case of pure-spin injection.

To explain the presence of the TSHE, we again refer to the four scenarios shown in Fig. 2(d). Within $-4.5J_{\mathrm{H}} < \epsilon_F < -J_{\mathrm{H}}$, the transport is dominated by scenario (I)+(III) as shown in Fig. 3(c). In this case, both the spin-up and spin-down electrons are injected from terminal 1. Due to the presence of a skyrmion there exists a topological Hall effect which produces a transverse electrical field, E_{TH}. At steady state, the zero-current

condition at terminals 2 and 4 requires $eE_{\mathrm{TH}} = -F \uparrow$ and $eE_{\mathrm{TH}} = -F \downarrow$ satisfied simultaneously. Due to the chirality of the skyrmion, the emergent field experienced by the up spin is opposite to that experienced by the down spin, which generates opposite emergent Lorentz forces on the two types of spins ($F \uparrow = -F \downarrow$). Therefore, the zero-current condition in the transverse direction cannot be satisfied unless $E_{\mathrm{TH}} = 0$. Although imbalanced spin injection occurs due to the ferromagnetic electrodes, the THE must be suppressed in steady state as long as the transport is dominated by the same type of carrier. Since there is no electrostatic field to balance the emergent Lorentz force, up-spin and down-spin carriers flow in opposite directions at the transverse terminals. Assuming the transverse terminals are coupled to perfect electrodes, the accumulated spins vanish quickly into the thermal bath. Thus, a continuous spin Hall current is established. Similar explanations [(II)+(IV)] can be applied for $J_{\mathrm{H}} < \epsilon_F < 4.5 J_{\mathrm{H}}$.

When the transport is dominated by two different types of carriers with the same spin, the TSHE is suppressed, and the THE voltage becomes finite. This occurs when ϵ_F is within the range $[-J_{\mathrm{H}}, J_{\mathrm{H}}]$, and the transport is dominated by the scenarios (II)+(III). In this case the down-spin electrons and holes are injected from terminals 1 and 3, respectively. The electrons and holes are scattered in opposite directions and then accumulate at terminals 2 and 4, respectively. Since the same spin is assigned to opposite charges, a non-zero E_{TH} develops at terminals (2) and (4) resulting in a finite THE with a vanishing TSHE.

To further demonstrate the differences between the THE and the TSHE, we show the vector map of the spin current density $\mathbf{J}_{S_z}(\mathbf{r})$ and the corresponding color map of the charge accumulation in Fig. 4. The spin texture and the terminal numbering are the same as in Fig. 1. For the THE case shown in Fig. 4(a), $\epsilon_F = -0.05 J_{\mathrm{H}}$ and the transport is dominated by scenario (II)+(III). There is a net drop in the transverse chemical potential between leads 2 and 4. The $\mathbf{J}_{S_z}$ vectors circulate symmetrically on either side of the skyrmion, generating no significant total transverse spin current. This corresponds to the case where $\theta_{\mathrm{TH}} \approx -0.2$ and $\theta_{\mathrm{TSH}} \approx 0$. For the TSHE case shown in [Fig. 4(b)], the transport is dominated by scenario (I)+(III). The equal-potential contour of $\delta\mu(\mathbf{r}) = 0$ cuts all the way across the vertical bar indicating little charge imbalance between leads 2 and 4. In transverse leads 2 and 4 there is a net spin current directed from lead 2 to lead 4 giving a negative $\theta_{\mathrm{TSH}} \approx -0.05$.

The TSHE discussed here is of similar magnitude as the SHE in widely used Pt thin films [31]. However, the physical mechanism giving rise to the TSHE is fundamentally different from the one leading to the spin Hall effect in strong spin orbit coupled systems. In such systems, the spin Hall effect results from the topological property of the Bloch bands in momentum space. In
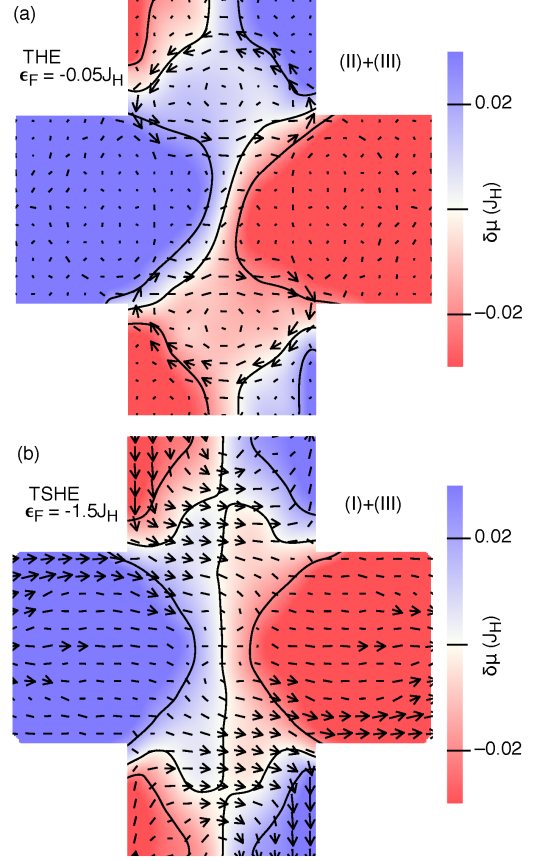

FIG. 4. (color online) Vector map of $\vec{J}_{S_z}$ (arrow plot) and the effective chemical potential distribution (color map) for (a) the THE and (b) the TSHE. A longitudinal applied bias of $\delta\mu_1 = -\delta\mu_3 = 0.1 J_{\mathrm{H}}$ is applied. For the THE (a), the spin current symmetrically circulates on either side of the skyrmion resulting in no net transverse spin current. The electron and hole accumulation induces an imbalanced transverse potential distribution. For the TSHE (b), the transverse chemical potential distribution is symmetric, and a charge-less spin current is established in the transverse direction.

contrast the TSHE results from the topological property of the skyrmion spin texture in real space. The real-space topology exerts opposite emergent Lorentz forces on different spins which can induce the TSHE.

* E-mail: gyin001@ucr.edu

[†] corresponding author; E-mail: jiadongzang@gmail.com
[‡] corresponding author; E-mail: rlake@ee.ucr.edu

[1] M. I. Dyakonov and V. I. Perel, Physics Letters A **35**, 459 (1971), ISSN 0375-9601, .

[2] M. I. Dyakonov and V. I. Perel, Sov. Phys. JETP Lett. **13**, 467 (1971), .

[3] A. A. Bakun, B. P. Zakharchenya, A. A. Rogachev, M. N. Tkachuk, and V. G. Fleisher, Sov. Phys. JETP Lett. (1984).

[4] M. N. Tkachuk, B. P. Zakharchenya, and V. G. Fleisher, Sov. Phys. JETP Lett. (1986).

[5] J. E. Hirsch, Phys. Rev. Lett. **83**, 1834 (1999), .

[6] S. Murakami, N. Nagaosa, and S.-C. Zhang, Science **301**, 1348 (2003), ISSN 0036-8075, 1095-9203, .

[7] J. Sinova, D. Culcer, Q. Niu, N. A. Sinitsyn, T. Jungwirth, and A. H. MacDonald, Phys. Rev. Lett. **92**, 126603 (2004), .

[8] B. K. Nikolić, S. Souma, L. P. Zârbo, and J. Sinova, Phys. Rev. Lett. **95**, 046601 (2005), .

[9] T. Grover and T. Senthil, Phys. Rev. Lett. **100**, 156804 (2008), .

[10] J. Iwasaki, M. Mochizuki, and N. Nagaosa, Nature Communications **4**, 1463 (2013), ISSN 2041-1723, .

[11] J. Wunderlich, B. Kaestner, J. Sinova, and T. Jungwirth, Phys. Rev. Lett. **94**, 047204 (2005), .

[12] Y. K. Kato, R. C. Myers, A. C. Gossard, and D. D. Awschalom, Science **306**, 1910 (2004), ISSN 0036-8075, 1095-9203, .

[13] J. Smit, Physica **21**, 877 (1955), ISSN 0031-8914, .

[14] L. Berger, Phys. Rev. B **2**, 4559 (1970), .

[15] M. Onoda and N. Nagaosa, J. Phys. Soc. Jpn. **71**, 19 (2002), ISSN 0031-9015, .

[16] N. Nagaosa, J. Sinova, S. Onoda, A. H. MacDonald, and N. P. Ong, Rev. Mod. Phys. **82**, 1539 (2010), .

[17] F. D. M. Haldane, Phys. Rev. Lett. **93**, 206602 (2004), .

[18] G. E. Volovik, in *AIP Conference Proceedings* (AIP Publishing, 1989), vol. 194, pp. 136–146, .

[19] Y. Taguchi, Y. Oohara, H. Yoshizawa, N. Nagaosa, and Y. Tokura, Science **291**, 2573 (2001), ISSN 0036-8075, 1095-9203, .

[20] P. Bruno, V. K. Dugaev, and M. Taillefumier, Phys. Rev. Lett. **93**, 096806 (2004), .

[21] X. Z. Yu, Y. Onose, N. Kanazawa, J. H. Park, J. H. Han, Y. Matsui, N. Nagaosa, and Y. Tokura, Nature **465**, 901 (2010), ISSN 0028-0836, .

[22] S. Mühlbauer, B. Binz, F. Jonietz, C. Pfleiderer, A. Rosch, A. Neubauer, R. Georgii, and P. Böni, Science **323**, 915 (2009), ISSN 0036-8075, 1095-9203, .

[23] T. Schulz, R. Ritz, A. Bauer, M. Halder, M. Wagner, C. Franz, C. Pfleiderer, K. Everschor, M. Garst, and A. Rosch, Nat Phys **8**, 301 (2012), ISSN 1745-2473, .

[24] Y. Li, N. Kanazawa, X. Z. Yu, A. Tsukazaki, M. Kawasaki, M. Ichikawa, X. F. Jin, F. Kagawa, and Y. Tokura, Phys. Rev. Lett. **110**, 117202 (2013), .

[25] N. Kanazawa, Y. Onose, T. Arima, D. Okuyama, K. Ohoyama, S. Wakimoto, K. Kakurai, S. Ishiwata, and Y. Tokura, Phys. Rev. Lett. **106**, 156603 (2011), .

[26] A. Neubauer, C. Pfleiderer, B. Binz, A. Rosch, R. Ritz, P. G. Niklowitz, and P. Böni, Phys. Rev. Lett. **102**, 186602 (2009), .

[27] S. X. Huang and C. L. Chien, Phys. Rev. Lett. **108**, 267201 (2012), .

[28] S. Datta, *Quantum Transport: Atom to Transistor* (Cambridge University Press, Cambridge, UK; New York, 2005), 2nd ed., ISBN 9780521631457.

[29] J. Iwasaki, M. Mochizuki, and N. Nagaosa, Nat Nano **8**, 742 (2013), ISSN 1748-3387, .

[30] G. Yin, Y. Li, L. Kong, R. K. Lake, C. L. Chien, and J. Zang, arXiv:1411.7762 [cond-mat] (2014), arXiv: 1411.7762, .

[31] L. Liu, T. Moriyama, D. C. Ralph, and R. A. Buhrman, Phys. Rev. Lett. **106**, 036601 (2011), .